Anisotropic Weyl Fermions from the Quasiparticle Excitation Spectrum of a 3D Fulde-Ferrell Superfluid

Yong Xu, Rui-Lin Chu, and Chuanwei Zhang*
Department of Physics, The University of Texas at Dallas, Richardson, Texas 75080, USA
(Received 28 October 2013; revised manuscript received 1 February 2014; published 31 March 2014)

Weyl fermions, first proposed for describing massless chiral Dirac fermions in particle physics, have not been observed yet in experiments. Recently, much effort has been devoted to explore Weyl fermions around band touching points of single-particle energy dispersions in certain solid state materials (named *Weyl semimetals*), similar as graphene for Dirac fermions. Here we show that such Weyl semimetals also exist in the quasiparticle excitation spectrum of a three-dimensional spin-orbit-coupled Fulde-Ferrell superfluid. By varying Zeeman fields, the properties of Weyl fermions, such as their creation and annihilation, number and position, as well as anisotropic linear dispersions around band touching points, can be tuned. We study the manifestation of anisotropic Weyl fermions in sound speeds of Fulde-Ferrell fermionic superfluids, which are detectable in experiments.

DOI: 10.1103/PhysRevLett.112.136402 PACS numbers: 71.10.Pm, 03.75.Lm, 05.30.Fk, 67.85.Lm

Introduction.—Weyl fermions [1] are massless chiral Dirac fermions with linear energy dispersions in momentum space. Recently, the existence of Weyl fermions has been explored in various solid state materials, such as pyrochlore iridates [2,3], ferromagnetic compound $HgCr_2Se_4$ [4], multilayer topological insulators [5], photonic crystals [6], as well as in optical lattices [7,8]. These materials, named Weyl semimetals, possess band touching points in their single-particle energy spectrum, around which the energy dispersions are linear and can be described by a chiral Weyl equation. These band touching points (i.e., Weyl nodes) appear in pairs with opposite topological invariance [9]. In contrast to two-dimensional (2D) Dirac fermions (e.g., graphene), which are unstable against perturbations that break time-reversal or spatial inversion symmetries, Weyl nodes are stable and the only way to destroy them is to merge two Weyl nodes with opposite topological invariances.

The recent progress in experimental observations of Majorana fermions (half of a regular Dirac fermion) using quasiparticle excitations in solid state topological superconductors [10–13] leads to a nature question: whether Weyl fermions can also be observed in the quasiparticle excitation spectrum (instead of single-particle spectrum) of superconductors or superfluids (e.g., ^{2}He A phase) [9,14,15]. While Majorana fermions in superconductors emerge as quasiparticle excitations in real space (inside defects) and low dimensions (1D or 2D), Weyl fermions describe energy dispersions in momentum space in three dimensions. Therefore, the semiconductor-superconductor heterostructures for observing Majorana fermions, where superconductivity is induced through proximity effects, are not suitable for the observation of Weyl fermions.

The recent experimental realization of spin-orbit (SO) coupling [16–21] in ultracold atomic gases provides another platform for exploring a variety of intriguing physics, including topological superfluids with Majorana fermions [22–29]. In particular, the low-temperature phase diagram of spin-orbit-coupled Fermi gases is dominated by Fulde-Ferrell (FF) superfluids with finite momentum pairing [30–40] in the presence of an in-plane Zeeman field, even in three dimensions. In one and two dimensions, such FF superfluids can support Majorana fermions [41–44]. However, whether such a FF superfluid state can support Weyl fermion excitations has not been explored.

In this Letter, we show that Weyl fermions can emerge from quasiparticle excitation spectrum of a 3D FF superfluid. The system we consider is a 3D degenerate Fermi gas with Rashba spin-orbit coupling (in the xy plane) and Zeeman fields [in-plane (h_x) and out-of-plane (h_z)]. The in-plane Zeeman field breaks the spatial inversion symmetry of the Fermi surface, yielding finite momentum pairing [32]. The rich phase diagrams in such 3D FF superfluids are obtained. In suitable parameter regions, we find band touching points between particle and hole branches in the quasiparticle excitation spectrum of the FF superfluid, which possess nonzero topological invariances and anisotropic linear dispersions along all three directions, indicating the existence of anisotropic Weyl fermion excitations. The properties of Weyl fermions, including their number and position, creation, and annihilation, and anisotropy, can be controlled by varying Zeeman fields and interaction strength between atoms. Finally, we investigate the signature of anisotropic Weyl fermion excitations in the speeds of sound of the FF fermionic superfluids, which are measurable in experiments.

Model and effective Hamiltonian.—We consider a 3D Fermi gas with s-wave contact interactions. The many-body Hamiltonian can be written as $H = \int d\mathbf{r}\hat{\Psi}^\dagger(\mathbf{r})H_s(\hat{\mathbf{p}})\hat{\Psi}(\mathbf{r}) - U\int d\mathbf{r}\hat{\Psi}^\dagger_\uparrow(\mathbf{r})\hat{\Psi}^\dagger_\downarrow(\mathbf{r})\hat{\Psi}_\downarrow(\mathbf{r})\hat{\Psi}_\uparrow(\mathbf{r})$, where the single-particle Hamiltonian $H_s(\hat{\mathbf{p}}) = (\hat{\mathbf{p}}^2/2m) - \mu + H_{\mathrm{SOC}}(\hat{\mathbf{p}}) + H_z$ with

momentum operator $\hat{\mathbf{p}} = -i\hbar\nabla$, chemical potential μ, attractive interaction strength U, and the atom mass m; the Rashba SO coupling $H_{\mathrm{SOC}}(\hat{\mathbf{p}}) = \alpha(\hat{\mathbf{p}} \times \sigma) \cdot \mathbf{e}_z$ with Pauli matrix σ; the Zeeman field is along the x (in-plane) and z (out-of-plane) directions, $H_z = h_x\sigma_x + h_z\sigma_z$. $\hat{\Psi}(\mathbf{r}) = [\hat{\Psi}_\uparrow(\mathbf{r}), \hat{\Psi}_\downarrow(\mathbf{r})]^T$ and $\hat{\Psi}^\dagger_\nu(\mathbf{r})$ $[\hat{\Psi}_\nu(\mathbf{r})]$ is the fermionic atom creation (annihilation) operator.

The thermodynamical potential in mean-field approximation can be written as

$$\Omega = |\Delta|^2/U + \sum_{\mathbf{k}} [\hbar^2(-\mathbf{k} + \mathbf{Q}/2)^2/2m - \mu] - \sum_{\mathbf{k},\sigma} \frac{1}{2\beta} \ln(1 + e^{-\beta E_{\mathbf{k}\sigma}}). \quad (1)$$

Here, $E_{\mathbf{k}\sigma}$ is the eigenvalue of the 4×4 Bogoliubov–de Gennes (BdG) Hamiltonian

$$H_B = \begin{pmatrix} H_s(\mathbf{k} + \mathbf{Q}/2) & \Delta_0 \\ \Delta_0 & -\sigma_y H_s(-\mathbf{k} + \mathbf{Q}/2)^* \sigma_y \end{pmatrix}, \quad (2)$$

$\mathbf{Q} = Q_y \mathbf{e}_y$ is the total momentum of the Cooper pair induced by the deformation of the Fermi surface [32]. The mean-field solutions of Δ_0, Q_y, and μ satisfy the saddle point equations $\partial\Omega/\partial\Delta_0 = 0$, $\partial\Omega/\partial Q_y = 0$, and the atom number equation $\partial\Omega/\partial\mu = -n$ with a fixed total atom density n. To regularize the ultraviolet divergence at large $\mathbf{k}$, we follow the standard procedure [45] $(1/U) = (m/4\pi\hbar^2 a_s) - \int (d\mathbf{k}/(2\pi)^3)(m/\hbar^2 k^2)$ with the s-wave scattering length a_s. The self-consistent solution is obtained through the minimization of the free energy $F = \Omega + \mu n$. The energy unit is chosen as the Fermi energy $E_F = \hbar^2 \mathbf{K}_F^2/2m$ of noninteracting Fermi gases without SO coupling and Zeeman fields with Fermi vector $K_F = (3\pi^2 n)^{1/3}$.

BCS-BEC crossover and phase diagram.—In Fig. 1, we plot the change of μ, Δ_0, and Q_y in the BCS-BEC crossover at zero temperature. With increasing $1/K_F a_s$, Δ_0 increases and μ decreases, signaling the crossover from BCS superfluids to BEC molecules. In the BEC limit, Δ_0, μ, and Q_y become the same for different values of (h_x, h_z) since fermion atoms form bound molecules. Henceforth, we focus on the BCS region. In this region, Δ_0 is smaller when the total Zeeman field $h = \sqrt{h_x^2 + h_z^2}$ is larger. The nonzero Q_y in the presence of h_x indicates the existence of Cooper pairings with finite center-of-mass momenta.

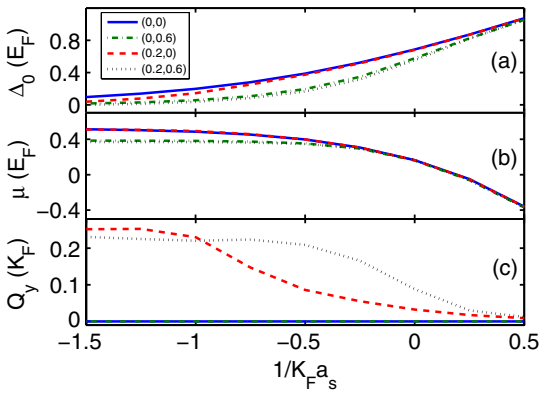

FIG. 1 (color online). Plot of Δ_0 in (a), μ in (b), and Q_y in (c) as a function of $1/K_F a_s$ for different parameters (h_x, h_z). $\alpha K_F = E_F$ and the temperature $T = 0$.

In Fig. 2(a), we map out the zero-temperature mean-field phase diagram in the (h_x, h_z) plane. In 3D Fermi gases, quantum fluctuations generally do not change the phase diagram qualitatively [46,47]. The uniform superfluid phase (with zero total momentum pairing), which exists at $h_x = 0$, is replaced by the gapped FF phase [36,37] in the presence of a small in-plane Zeeman field h_x because of the broken inversion symmetry of the Fermi surface. To characterize different phases, we consider the quasiparticle gap E_g that represents the energy difference between the minimum of the particle branch and the maximum of the hole branch ($E_g > 0$, gapped; $E_g \leq 0$, gapless). The topological FF (TFF) phase that supports Weyl fermions in the quasiparticle excitation spectrum appears in the large h_z region. The topological FF phase is gapped except at Weyl nodes, where $E_g = 0$. The critical h_z for the transition to the TFF phase decreases as h_x increases and reaches the minimum $h_z = 0.14E_F$ at $h_x = 0.45E_F$. In the absence of h_z, the gapless FF phase appears with a large range of h_x [36,37], while the region is extremely small [shown in the inset of Fig. 2(a)] in the presence of h_z. Instead, a new phase called gapless topological FF phase dominates the remaining parameter region because of the large total Zeeman field. This phase possesses nontopological gapless excitations in addition to topological Weyl fermions, which

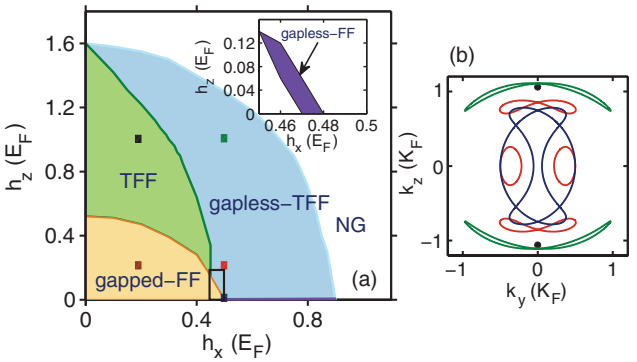

FIG. 2 (color). (a) Mean-field phase diagrams of 3D spin-orbit-coupled Fermi gases. The area in the small black box is enlarged in the inset, which shows the gapless FF phase. NG: Normal gas. (b) Contours of the zero energy quasiparticle spectrum in the plane (k_y, k_z) with $k_x = 0$. Here, $h_x = 0.5E_F$, $h_z = 0$ (blue line), $h_z = 0.2E_F$ (red line), $h_z = E_F$ (green line), and $h_x = 0.2E_F$, $h_z = E_F$ (black points) correspond to blue, red, green, and black square points in (a). The brown point in the gapped FF phase has no zero energy excitations. In both figures, $\alpha K_F = E_F$ and $1/a_s K_F = -0.1$.

is different from the topological FF phase where Weyl nodes are the only gapless excitations. This phase should also be distinguished from the gapless FF state because its band structure has a certain topological property.

Topological FF phase.—The transition from the gapped FF phase to topological FF phase is characterized by the quasiparticle excitation gap that closes and reopens with increasing h_z for a fixed k_z and a small h_x. During this transition, the minimum of the band gap E_g occurs at $k_x = k_y = 0$, and the gap closes when

$$(h_x + \alpha Q_y/2)^2 + h_z^2 = (\hbar^2 k_z^2/2m - \mu)^2 + \Delta_0^2, \quad (3)$$

which determines the position $\mathbf{k}_W = (0, 0, k_c)$ of the Weyl nodes. Such gap close and reopening is shown in Fig. 3(a) for $k_z = 0$. During this transition, the order parameter Δ_0 is still finite even though the bulk gap is closed. The finite Q_y indicates the FF superfluid. In Fig. 3(b), we plot the Weyl nodes determined by Eq. (3) in the (k_z, h_z) plane. For a fixed h_z and h_x, the superfluid is topological when Weyl nodes exist at certain k_z. There are two topological regions: $h_z > \sqrt{\mu^2 + \Delta_0^2 - (h_x + \alpha Q_y/2)^2}$ with two Weyl nodes and $\sqrt{\Delta_0^2 - (h_x + \alpha Q_y/2)^2} < h_z < \sqrt{\mu^2 + \Delta_0^2 - (h_x + \alpha Q_y/2)^2}$ with four Weyl nodes. Both critical values for h_z decrease with increasing h_x. To confirm such excitations are Weyl fermions, we examine the energy dispersions around these node points and find they are linear but with different slopes along different directions [see Fig. 4(a)]. While the different slopes between k_z and in-plane directions are due to the 2D SO coupling, the difference between the k_x and k_y directions is caused by the finite momentum Q_y of the Cooper pairs induced by h_x. From Eq. (3), we see the properties of Weyl fermions, such as position (k_c), number (2 or 4), and their creation and annihilation, can be tuned by varying h_z and h_x. Note that the anisotropy of Weyl fermions can also be tuned by the external magnetic field in solid materials (e.g., pyrochlore iridates [3]). In addition, such Weyl fermions appear in pairs with opposite topological charges $N_c = \pm 1$ [48].

Weyl nodes can also be regarded as quantum Hall transition points in the momentum space parametrized by k_z. In the topological FF phase, because the quasiparticle excitations are gapped (except at the Weyl nodes) in the 2D plane with a fixed k_z, we can calculate the Chern number for the hole branch for each k_z plane

$$C(k_z) = \frac{1}{2\pi} \sum_n \int dk_x dk_y \Omega^n(k_x, k_y), \quad (4)$$

where n is the index for hole branches, and the Berry curvature [50]

$$\Omega^n = i \sum_{n' \neq n} \left[\frac{\langle n|\partial_{k_x} H_B|n'\rangle\langle n'|\partial_{k_y} H_B|n\rangle - (k_x \leftrightarrow k_y)}{(E_{n\mathbf{k}} - E_{n'\mathbf{k}})^2} \right], \quad (5)$$

and n', which is not equal to n, runs over the eigenstates of H_B. For the topological FF phase with two Weyl nodes, we find that $C = 1$ when $|k_z| < k_c$ and $C = 0$ when $|k_z| > k_c$ [see Fig. 3(c)]. For the topological FF phase with four Weyl nodes, $C = 1$ when k lies between two nodes in the positive

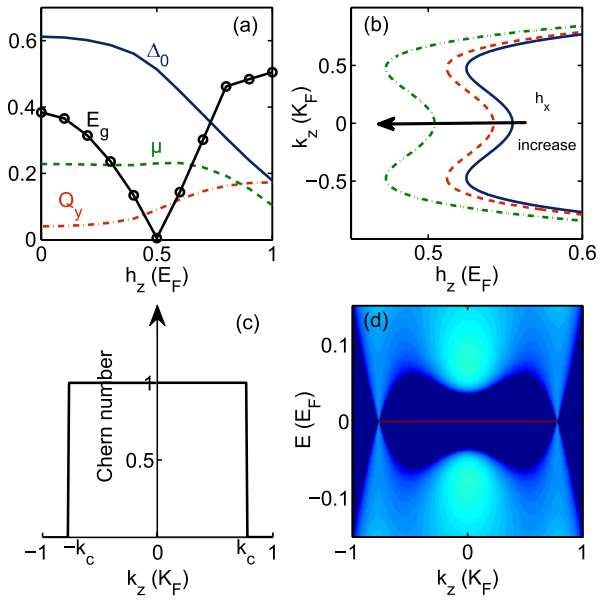

FIG. 3 (color online). (a) The change of the quasiparticle excitation gap E_g, Δ_0, Q_y, μ as a function of h_z with $h_x = 0.2E_F$. (b) Gap closing points ($E_g = 0$) in the (h_z, k_z) plane for $h_x = 0$ (solid blue line), $h_x = 0.1$ (dashed red line), and $h_x = 0.2$ (dashed-dotted green line). (c) Chern number for a fixed k_z plane. (d) Display of the density of states, which is calculated via the iterative Green function method [49], $k_y = 0$. The light blue region and the red line (Fermi arch) represent bulk and surface excitations, respectively. In (c) and (d), $h_x = 0.2E_F$, $h_z = 0.55E_F$. In all four figures $\alpha K_F = E_F$, $1/a_s K_F = -0.1$.

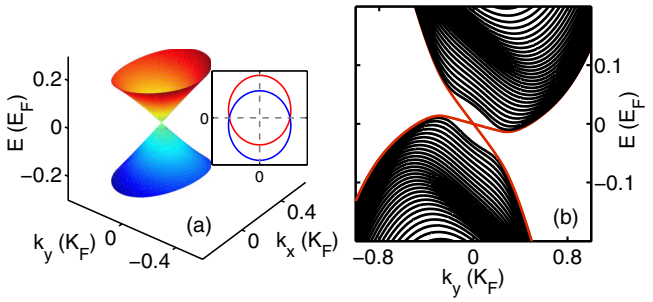

FIG. 4 (color online). (a) Quasiparticle excitations around the Weyl node $\mathbf{k}_W = (0, 0, 0.77K_F)$ with $h_z = 0.55E_F$ and $h_x = 0.2E_F$. The inset gives the contours of energy with $E = 0.1E_F$ (red line) and $E = -0.1E_F$ (blue line). (b) Quasiparticle excitation spectrum in the gapless topological FF phase as a function of k_y with fixed $k_z = 0.8K_F$ and confinement in the x direction. Black lines are bulk states while the red lines correspond to the surface state. $h_x = 0.5E_F$ and $h_z = 0.2E_F$. $\alpha K_F = E_F$, $1/a_s K_F = -0.1$ for both (a) and (b).

or negative k_z, and $C = 0$ otherwise. The Fermi surface lies at zero energy, which is composed of separated Weyl nodes. It is expected that there exist chiral edge states [2,4] in the presence of real space confinement along the x or y direction for a fixed k_z with nonzero Chern number. For instance, with the confinement along the x direction, there are two chiral edge states whose spectra intersect at $k_y = 0$ and $E = 0$ (k_z is already taken as a parameter). The zero energy Fermi surface now becomes a line (i.e., Fermi arc) in the (k_y, k_z) plane that connects two Weyl nodes [Fig. 3(d)].

Gapless topological FF phase.—Topological FF state is gapless by itself, but the gapless points occur only when particle and hole branches touch. With increasing h_x, the quasiparticle excitation spectrum becomes more asymmetric along the k_y direction. Above certain h_x, certain parts of the particle branch of the spectrum may fall below the zero energy, leading to a gapless FF phase with $E_g < 0$. Note that the band minimum of particle branch and maximum of hole branch do not occur at the same $\mathbf{k}$ in this phase. The gapless FF phase can be either nontopological or topological, depending on whether the particle and hole branches touch at certain $\mathbf{k}_W = (0, 0, k_c)$ with the linear dispersion. Figure 2(b) displays the zero energy contours in the (k_y, k_z) plane with $k_x = 0$ for different states. The topological FF phase has separate zero points along the k_z axis, while other phases have closed loops. For the gapless FF phase, the closed lines are connected. For the gapless topological FF phase, the particle and hole branch can still touch at certain $\mathbf{k}_W$. Instead of a single point, the zero energy contour now cuts close loops in the (k_x, k_y) plane and these loops are connected at $\mathbf{k}_W$. Away from $\mathbf{k}_W$ along the k_z direction, particle-hole branches do not touch, and the loops in the (k_x, k_y) plane are disconnected, which can be clearly seen from the bulk spectrum in Fig. 4(b). In the (k_y, k_z) plane with $k_x = 0$, it forms two connected loop structures around $\mathbf{k}_W$, as shown in Fig. 2(b). To confirm the topological nontrivial feature, we calculate the Chern number of the two hole bands and find it is one between two Weyl nodes and zero otherwise. Figure 4(b) shows the edge state (red line) in the gapless topological FF phase.

Sound speed of FF superfluids.—The anisotropic Weyl fermions in the topological FF phase have two characteristic properties: (i) the anisotropic energy spectrum along all three directions. Furthermore, the spectrum is different even for the $\pm k_y$ direction, which is special for the FF type of superfluids. (ii) The energy gap closes above a critical h_z for the topological phase transition. In experiments, the finite momentum pairing of the Cooper pairs may be measured using noise-correlation imaging [51] or momentum-resolved radio-frequency spectroscopy [35]. Here we propose the above two characteristic properties of Weyl fermions should manifest in the sound speeds of the underlying FF fermionic superfluids, which can be probed by observing the propagation of a localized density perturbation created by a laser beam, as demonstrated in previous experiments [52,53]. The sound speed can be obtained by calculating Gaussian fluctuations around the saddle point (Δ_0, Q_y) of the thermodynamical potential. Specifically, the speed of sound along the η direction is defined as $v_\eta = |\lim_{q\to 0}\partial\omega(q)/\partial q_\eta|$, where $\omega(q)$ is the bosonic gapless collective excitation spectrum [54] (see Supplemental Material [55]). Around the Weyl nodes, where the quasiparticle gap closes, we expect a sharp change of the sound speed because of the strong fluctuations around the phase transition points. In Fig. 5, we see the speeds of sound v_i are anisotropic along all three different directions, indicating anisotropic quasiparticle spectrum. More interestingly, the sound speeds along the positive and negative y directions are also different, indicating asymmetric spectrum along the y direction due to the finite momentum Cooper pairing. v_i has the minimum at the topological phase transition boundary [see Fig. 2(a)] to the topological FF phase with Weyl fermions. Therefore, we conclude that such anisotropic speeds of sound and the minimum located at the phase transition boundary provide strong evidence of Weyl fermions in a FF superfluid. In experiments, we consider a typical parameter with ^{40}K atoms and density $n = 5\times 10^{12}\,\mathrm{cm}^{-3}$, yielding the Fermi energy $E_F = h \times 3.5$ KHz and Fermi velocity $v_F = 8.3$ mm/s. The SO coupling and Zeeman field can be created by Raman coupling between atomic hyperfine states. The strength of the Zeeman field may be tuned by the detuning and intensity of Raman lasers [16–21,56].

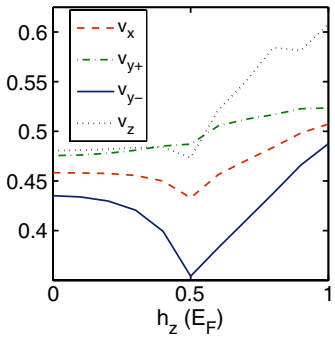

FIG. 5 (color online). Sound speeds as a function of h_z. Dashed red and dotted black lines represent the speed along the x and z directions. Solid blue and dashed-dot green lines represent sound speeds along the negative y and positive y directions, respectively. The unit of sound speed is $v_F = \hbar K_F/m$. Here, $h_x = 0.2E_F$, $\alpha K_F = E_F$, and $1/a_s K_F = -0.1$.

We would like to thank Xuele Liu, Li Mao, Lin Dong, and Ying Hu for helpful discussion and critical comments. This work is supported by ARO (W911NF-12-1-0334), AFOSR (FA9550-13-1-0045), and NSF-PHY (1249293).

*Corresponding author.
chuanwei.zhang@utdallas.edu

[1] H. Weyl, Z. Phys. **56**, 330 (1929).

[2] X. Wan, A. M. Turner, A. Vishwanath, and S. Y. Savrasov, Phys. Rev. B **83**, 205101 (2011).
[3] V. Aji, Phys. Rev. B **85**, 241101(R) (2012).
[4] G. Xu, H. Weng, Z. Wang, X. Dai, and Z. Fang, Phys. Rev. Lett. **107**, 186806 (2011).
[5] A. A. Burkov and L. Balents, Phys. Rev. Lett. **107**, 127205 (2011).
[6] L. Lu, L. Fu, J. D. Joannopoulos, and M. Soljačić, Nat. Photonics **7**, 294 (2013).
[7] D. Bercioux, D. F. Urban, H. Grabert, and W. Häusler, Phys. Rev. A **80**, 063603 (2009).
[8] Z. Lan, N. Goldman, and P. Öhberg, Phys. Rev. B **85**, 155451 (2012).
[9] G. E. Volovik, *The Universe in a Helium Droplet* (Clarendon Press, Oxford, 2003).
[10] V. Mourik, K. Zuo, S. M. Frolov, S. R. Plissard, E. P. A. M. Bakkers, and L. P. Kouwenhoven, Science **336**, 1003 (2012).
[11] M. T. Deng, C. L. Yu, G. Y. Huang, M. Larsson, P. Caroff, and H. Q. Xu, Nano Lett. **12**, 6414 (2012).
[12] A. Das, Y. Ronen, Y. Most, Y. Oreg, M. Heiblum, and H. Shtrikman, Nat. Phys. **8**, 887 (2012).
[13] L. P. Rokhinson, X. Liu, and J. K. Furdyna, Nat. Phys. **8**, 795 (2012).
[14] M. Gong, S. Tewari, and C. Zhang, Phys. Rev. Lett. **107**, 195303 (2011).
[15] K. Seo, C. Zhang, and S. Tewari, Phys. Rev. A **87**, 063618 (2013).
[16] Y.-J. Lin, K. Jiménez-García, and I. B. Spielman, Nature (London) **471**, 83 (2011).
[17] P. Wang, Z.-Q. Yu, Z. Fu, J. Miao, L. Huang, S. Chai, H. Zhai, and J. Zhang, Phys. Rev. Lett. **109**, 095301 (2012).
[18] L. W. Cheuk, A. T. Sommer, Z. Hadzibabic, T. Yefsah, W. S. Bakr, and M. W. Zwierlein, Phys. Rev. Lett. **109**, 095302 (2012).
[19] J.-Y. Zhang, S.-C. Ji, Z. Chen, L. Zhang, Z.-D. Du, B. Yan, G.-S. Pan, B. Zhao, Y.-J. Deng, H. Zhai, S. Chen, and J.-W. Pan, Phys. Rev. Lett. **109**, 115301 (2012).
[20] C. Qu, C. Hamner, M. Gong, C. Zhang, and P. Engels, Phys. Rev. A **88**, 021604(R) (2013).
[21] R. A. Williams, M. C. Beeler, L. J. LeBlanc, K. Jiménez-García, and I. B. Spielman, Phys. Rev. Lett. **111**, 095301 (2013).
[22] C. Zhang, S. Tewari, R. M. Lutchyn, and S. Das Sarma, Phys. Rev. Lett. **101**, 160401 (2008).
[23] M. Sato, Y. Takahashi, and S. Fujimoto, Phys. Rev. Lett. **103**, 020401 (2009).
[24] S.-L. Zhu, L.-B. Shao, Z. D. Wang, and L.-M. Duan, Phys. Rev. Lett. **106**, 100404 (2011).
[25] L. Jiang, T. Kitagawa, J. Alicea, A. R. Akhmerov, D. Pekker, G. Refael, J. I. Cirac, E. Demler, M. D. Lukin, and P. Zoller, Phys. Rev. Lett. **106**, 220402 (2011).
[26] X.-J. Liu, and H. Hu, Phys. Rev. A **85**, 033622 (2012).
[27] K. Seo, L. Han, and C. A. R. Sá de Melo, Phys. Rev. Lett. **109**, 105303 (2012).
[28] M. Gong, G. Chen, S. Jia, and C. Zhang, Phys. Rev. Lett. **109**, 105302 (2012).
[29] X.-J. Liu, K. T. Law, and T. K. Ng, arXiv:1304.0291 [Phys. Rev. Lett. (to be published)].
[30] P. Fulde, and R. A. Ferrell, Phys. Rev. **135**, A550 (1964).
[31] A. I. Larkin, and Yu. N. Ovchinnikov, Zh. Eksp. Teor. Fiz. **47**, 1136 (1964) [Sov. Phys. JETP **20**, 762 (1965)].
[32] Z. Zheng, M. Gong, X. Zou, C. Zhang, and G. Guo, Phys. Rev. A **87**, 031602(R) (2013).
[33] F. Wu, G.-C. Guo, W. Zhang, and W. Yi, Phys. Rev. Lett. **110**, 110401 (2013).
[34] X.-J. Liu and H. Hu, Phys. Rev. A **87**, 051608(R) (2013).
[35] Z. Fu, L. Huang, Z. Meng, P. Wang, X.-J. Liu, H. Pu, H. Hu, and J. Zhang, Phys. Rev. A **87**, 053619 (2013).
[36] L. Dong, L. Jiang, and H. Pu, New J. Phys. **15**, 075014 (2013).
[37] H. Hui and X.-J. Liu, New J. Phys. **15**, 093037 (2013).
[38] M. Iskin, Phys. Rev. A **88**, 013631 (2013).
[39] Y. Xu, C. Qu, M. Gong, and C. Zhang, Phys. Rev. A **89**, 013607 (2014).
[40] X.-J. Liu, Phys. Rev. A **88**, 043607 (2013).
[41] C. Qu, Z. Zheng, M. Gong, Y. Xu, L. Mao, X. Zou, G. Guo, and C. Zhang, Nat. Commun. **4**, 2710 (2013).
[42] W. Zhang and W. Yi, Nat. Commun. **4**, 2711 (2013).
[43] X.-J. Liu and H. Hu, Phys. Rev. A **88**, 023622 (2013).
[44] C. Chen, Phys. Rev. Lett. **111**, 235302 (2013).
[45] S. Giorgini, L. P. Pitaevskii, and S. Stringari, Rev. Mod. Phys. **80**, 1215 (2008).
[46] L. He, X.-G. Huang, H. Hu, and X.-J. Liu, Phys. Rev. A **87**, 053616 (2013).
[47] J. P. A. Devreese and J. Tempere, Phys. Rev. A **89**, 013616 (2014).
[48] The topological charge is defined as $N_c = (1/24\pi^2) e_{\mu\nu\lambda\gamma} \mathrm{tr} \int_{\sum_a} dS^\gamma \mathcal{G}\partial_{p_\mu}\mathcal{G}^{-1}\mathcal{G}\partial_{p_\nu}\mathcal{G}^{-1}\mathcal{G}\partial_{p_\lambda}\mathcal{G}^{-1}$ [9], where the Green function $\mathcal{G}^{-1} = ik_0 - H_B(\mathbf{k})$, the integral is over the 3D surface $\sum_c$ embracing the isolated Weyl node $\mathbf{k}_W = (0, 0, k_c)$, and tr stands for the trace in the spin space.
[49] X. Dai, T. L. Hughes, X.-L. Qi, Z. Fang, and S.-C. Zhang, Phys. Rev. B **77**, 125319 (2008).
[50] D. Xiao, M.-C. Chang, and Q. Niu, Rev. Mod. Phys. **82**, 1959 (2010).
[51] M. Greiner, C. A. Regal, J. T. Stewart, and D. S. Jin, Phys. Rev. Lett. **94**, 110401 (2005).
[52] M. R. Andrews, D. M. Kurn, H.-J. Miesner, D. S. Durfee, C. G. Townsend, S. Inouye, and W. Ketterle, Phys. Rev. Lett. **79**, 553 (1997).
[53] J. Joseph, B. Clancy, L. Luo, J. Kinast, A. Turlapov, and J. E. Thomas, Phys. Rev. Lett. **98**, 170401 (2007).
[54] J. R. Engelbrecht, M. Randeria, and C. A. R. Sáde Melo, Phys. Rev. B **55**, 15153 (1997).
[55] See Supplemental Material at http://link.aps.org/supplemental/10.1103/PhysRevLett.112.136402 for calculation of sound speeds.
[56] C. Zhang, Phys. Rev. A **82**, 021607(R) (2010).